

Reshaping nonclassical properties and metrological performance of entangled coherent states via post-selected von Neumann measurements

Janarbek Yuanbek^{1,2,4§}, Bruno Tenorio^{3§} and Yusuf Turek^{4*}

¹State Key Laboratory of Semiconductor Physics and Chip Technologies,
Institute of Semiconductors, Chinese Academy of Sciences, Beijing 100083, China

²Center of Materials Science and Opto-Electronic Technology,
University of Chinese Academy of Sciences, Beijing 100049, China

³Wolfram Research South America, Lima 15076, Peru *and*

⁴School of Physics, Liaoning University, Shenyang, Liaoning 110036, China

(Dated: April 21, 2026)

In quantum metrology, measurements are usually treated as passive readout processes. Here we investigate whether post-selected von Neumann measurements (PVNMs) can be used as an active resource to reshape the nonclassical properties of a two-mode entangled coherent state (ECS). By analyzing the finite-coupling post-selected state, we show that PVNMs can enhance quadrature squeezing and sum squeezing, increase the Wigner-function negativity, and strengthen bipartite correlations, as witnessed by the Hillery–Zubairy criterion and linear entropy. We further evaluate the quantum Fisher information and the corresponding quantum Cramér–Rao bound for phase estimation, and discuss the trade-off between metrological gain and measurement-induced disturbance through the fidelity. Our scheme exhibits a phase-sensitivity advantage over standard ECS metrology for large average photon numbers. Our results suggest that PVNMs provide a tunable route for engineering nonclassical resources in continuous-variable sensing protocols.

I. INTRODUCTION

Quantum metrology [1] has become a central topic in quantum optics because it offers the possibility of parameter estimation beyond classical limits, by exploiting nonclassical resources such as entanglement and interference [2]. A variety of probe states have been proposed for this purpose, including NOON states [3, 4], “bat” states [5], and entangled coherent states (ECS) [6–8]. Among these, ECS have been shown to offer competitive phase-estimation sensitivity compared with NOON states, “bat” states, and uncorrelated states at the same average photon number, while also exhibiting favorable robustness to losses in certain regimes. These advantages are commonly quantified using the quantum Fisher information, which provides a fundamental bound on the achievable precision in parameter estimation.

Despite these advances, existing analyses are predominantly based on standard measurement paradigms, where the role of measurement is treated as passive and does not fundamentally alter the structure of the probe state [9, 10]. This assumption may become inadequate when considering weak measurement protocols, in which measurement itself can actively reshape the statistical and coherence properties of quantum systems. Within this framework, pre-selection, post-selection, and weak system–pointer coupling jointly enable information extraction with limited disturbance, giving rise to weak values that may lie outside the eigenvalue spectrum and can be used for signal amplification in appropriate regimes [11–14]. Such features have been successfully exploited in single-mode settings [15] and have been suggested to influence quantum statistical properties

[16–18] more generally, indicating that weak measurements may offer capabilities beyond those captured by conventional metrological approaches.

However, how these measurement-induced effects extend to entangled states remains less explored. In particular, the non-destructive manipulation of nonclassical features in ECS poses a significant challenge for practical implementations. The presence of post-selection can substantially modify measurement statistics and quantum correlations, potentially leading to regimes where precision limits deviate from those predicted by standard quantum Fisher information analysis [19–21]. Understanding this interplay is therefore essential for determining whether weak measurement can enhance, preserve, or even degrade the metrological advantages of ECS. Motivated by these considerations, it is crucial to establish a systematic framework for analyzing post-selected von Neumann measurements (PVNMs) [22] acting on ECS. Such an investigation not only clarifies the role of measurement in quantum metrology but also opens the possibility of leveraging weak measurement as an active resource for optimizing quantum sensing protocols beyond conventional paradigms.

Unlike previous weak-value amplification studies that mainly focus on anomalous pointer shifts and parameter estimation, the present work investigates how post-selected von Neumann measurements reshape the nonclassical properties of entangled coherent states. In this work, we study PVNMs applied to a two-mode ECS and analyze their influence on squeezing, Wigner-function negativity, entanglement, and phase-estimation performance. By tuning the system–pointer coupling strengths, we show that PVNMs can modify the quantum state in a controllable manner, which in certain parameter regimes leads to enhanced quadrature and sum squeezing, increased Wigner negativity, and stronger bipartite entanglement as quantified by the Hillery–Zubairy criterion and linear entropy. We further examine the quantum Fisher information and the corresponding

§ These authors contributed equally to this work.

* Corresponding author: yusufu1984@hotmail.com

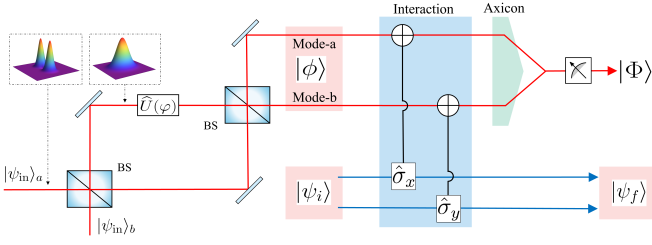


Figure 1. Schematic illustration of ECS preparation and PVNMs. An ECS is generated by interfering coherent inputs at a 50:50 beam splitter and applying the phase shift $\hat{U}(\varphi)$. The system is then pre-selected in $|\psi_i\rangle$, interacts with the pointer, and is post-selected in $|\psi_f\rangle$, yielding the final pointer state $|\Phi\rangle$.

quantum Cramér–Rao bound, showing that the measurement-induced modification can improve phase sensitivity within the explored parameter regime. Compared with standard ECS metrology [6], our post-selected scheme achieves a distinct phase-sensitivity advantage for large average photon numbers. At the same time, fidelity analysis reveals the expected trade-off between resource enhancement and state disturbance.

The paper is organized as follows. In Sec. II, we construct the theoretical model using the PVNMs framework and derive the final pointer state. Sec. III, we employ this model to analyze the effects of PVNMs on the quadrature and sum squeezing properties of the entangled coherent state. In Sec. IV, we examine the measurement back-action in phase space by studying the evolution of the joint and single-mode Wigner functions. In Sec. V, we quantify the modification of two-mode entanglement using the Hillery-Zubairy criterion and linear entropy. In Sec. VI, we assess the metrological utility of the enhanced state by calculating the quantum Fisher information. In Sec. VII, we analyze the fidelity between the initial and post-selected pointer states. In Sec. VIII, we briefly discuss the influence of open system effects on the dynamics. Finally, in Sec. IX, we summarize the key findings and provide an outlook for future research. Throughout the paper, we set $\hbar = 1$.

II. THEORETICAL FRAMEWORK

ECS are nonclassical states that arise from the superposition of coherent light fields across various spatial modes, combining the experimental accessibility of coherent states with intrinsically quantum entanglement properties [23]. As illustrated in Fig. 1, an ECS can be generated by injecting an even cat state $|\psi_{in}\rangle_a = \mathcal{N}(|\alpha/\sqrt{2}\rangle + |-\alpha/\sqrt{2}\rangle)$ [24], where $\mathcal{N} = [2(1 + e^{-2|\alpha|^2})]^{-1/2}$ is the normalization factor [25] and a coherent state $|\psi_{in}\rangle_b = |\alpha/\sqrt{2}\rangle$ into the two input ports of a 50:50 beam splitter (BS) [6, 26]. After the unitary transformation implemented by the beam splitter, is given by $|\phi_{in}\rangle = |\psi_{in}\rangle_a \otimes |\psi_{in}\rangle_b = \mathcal{N}(|\alpha\rangle_a|0\rangle_b + |0\rangle_a|\alpha\rangle_b)$. Here, $\alpha = re^{i\mu}$, and $|0\rangle$ and $|\alpha\rangle$ denote the vacuum and coherent states in spatial modes a and b , respectively. To study phase sensing, we apply a phase shift to mode b through $\hat{U}(\varphi) = \mathbb{I} \otimes e^{i\varphi\hat{n}_b}$, where $\hat{n}_b = \hat{b}^\dagger\hat{b}$ is the photon-number operator of mode b , and \mathbb{I} denotes the identity operator acting

on mode a . The action of this operation on a coherent state is given by $e^{i\varphi\hat{n}_b}|\alpha\rangle_b = |\alpha e^{i\varphi}\rangle_b$. Finally, the output ECS is obtained as

$$|\phi\rangle = \hat{U}(\varphi)|\phi_{in}\rangle = \mathcal{N}(|\alpha\rangle_a|0\rangle_b + |0\rangle_a|\alpha e^{i\varphi}\rangle_b). \quad (1)$$

For simplicity, this work analyzes the impact of PVNMs on the properties of ECS and their applications in quantum precision measurement, where the total system pointer Hamiltonian is decomposed into three fundamental terms governing distinct physical processes during the interaction. The total Hamiltonian is written as

$$\hat{H} = \hat{H}_s + \hat{H}_p + \hat{H}_{int}, \quad (2)$$

where \hat{H}_s and \hat{H}_p describe the system and pointer, respectively, and \hat{H}_{int} describes their interaction. Within ideal measurement theory, the choice of \hat{H}_s and \hat{H}_p is inconsequential to the outcomes; only \hat{H}_{int} determines the measurement strength and post-selection statistics. Without loss of generality, the interaction Hamiltonian is chosen as [27]

$$\hat{H}_{int} = g_a\hat{\sigma}_x \otimes \hat{P}_x + g_b\hat{\sigma}_y \otimes \hat{P}_y, \quad (3)$$

where g_a and g_b are the system–pointer coupling strengths. The measured observables $\hat{\sigma}_x$ and $\hat{\sigma}_y$ are expressed in their respective eigenbases as

$$\hat{\sigma}_x = |H\rangle\langle V| + |V\rangle\langle H|, \quad (4)$$

$$\hat{\sigma}_y = i|V\rangle\langle H| - i|H\rangle\langle V|, \quad (5)$$

where $|H\rangle$ and $|V\rangle$ denote the horizontal and vertical polarization states. The pointer momenta \hat{P}_x and \hat{P}_y are conjugate to the pointer quadratures \hat{X} and \hat{Y} , satisfying $[\hat{X}, \hat{P}_x] = [\hat{Y}, \hat{P}_y] = i$. Both operators can be expressed via annihilation (\hat{a} , \hat{b}) and creation (\hat{a}^\dagger , \hat{b}^\dagger) operators as $\hat{P}_x = i(\hat{a}^\dagger - \hat{a})/2\sigma$ and $\hat{P}_y = i(\hat{b}^\dagger - \hat{b})/2\sigma$ [28], where $\sigma = \sqrt{1/2m\omega}$ is the ground-state width of the pointer, determined by its mass m and oscillation frequency ω . As shown in Fig. 1, we illustrate the experimental setup of weak interactions. Based on this, the initial composite state is given by

$$|\Psi_{in}\rangle = |\psi_i\rangle \otimes |\phi\rangle. \quad (6)$$

Here the initial system state is prepared as $|\psi_i\rangle = \cos(\theta/2)|H\rangle + e^{i\delta}\sin(\theta/2)|V\rangle$, where $\delta \in [0, 2\pi]$ and $\theta \in [0, \pi]$. In a PVNMs, the system is defined by both pre- and post-selection of its state. We prepare the system in an initial state $|\psi_i\rangle$ and then we couple it to the pointer state. After some interaction time t , we post-select a system state $|\psi_f\rangle$, and obtain information on the physical quantities $\hat{\sigma}_x$ and $\hat{\sigma}_y$ from the pointer wave function. For definiteness, we set the post-selected state to $|\psi_f\rangle = |H\rangle$. The interaction acts for a finite duration t , so the unitary evolution generated by H_{int} is

$$\hat{U}(t) = e^{-i\int_0^t H_{int} dt'} = e^{-itg_a\hat{\sigma}_x \otimes \hat{P}_x - ig_bt\hat{\sigma}_y \otimes \hat{P}_y}, \quad (7)$$

Since the operators $\hat{\sigma}_x$ and $\hat{\sigma}_y$ satisfy $\hat{\sigma}_x^2 = \hat{\sigma}_y^2 = \mathbb{I}$, the evolution operators can be written as:

$$e^{-igat\hat{\sigma}_x\otimes\hat{P}_x} = \frac{1}{2} \left[\Upsilon_+ \otimes D_1\left[\frac{s_1}{2}\right] + \Upsilon_- \otimes D_1^\dagger\left[\frac{s_1}{2}\right] \right], \quad (8)$$

$$e^{-igbt\hat{\sigma}_y\otimes\hat{P}_y} = \frac{1}{2} \left[\Upsilon'_+ \otimes D_2\left[\frac{s_2}{2}\right] + \Upsilon'_- \otimes D_2^\dagger\left[\frac{s_2}{2}\right] \right], \quad (9)$$

where $\Upsilon_\pm = \mathbb{I} \pm \hat{\sigma}_x$ and $\Upsilon'_\pm = \mathbb{I} \pm \hat{\sigma}_y$. The displacement operator is defined by $D(\alpha) = \exp[\alpha\hat{a}^\dagger - \alpha^*\hat{a}]$, and the coupling strength parameter is $s_1 = gat/\sigma$, and $s_2 = gbt/\sigma$. For real $s_{1,2}$ this yields $D_1[s_1/2] = \exp[s_1(\hat{a}^\dagger - \hat{a})/2]$ and $D_2[s_2/2] = \exp[s_2(\hat{b}^\dagger - \hat{b})/2]$. After the interaction, the initial state becomes

$$|\Psi\rangle = \hat{U}(t) |\Psi_{in}\rangle. \quad (10)$$

In PVMs, the state $|\Psi\rangle$ is projected onto the post-selected state $|\psi_f\rangle$, yielding an unnormalized pointer state $|\tilde{\Phi}\rangle = \langle\psi_f|\Psi\rangle$. The final normalized probe state is given by

$$\begin{aligned} |\Phi\rangle &= \frac{|\tilde{\Phi}\rangle}{\sqrt{P_s}} \\ &= \frac{\kappa}{4} \left\{ A_+ D_1\left[\frac{s_1}{2}\right] D_2\left[\frac{s_2}{2}\right] + A_- D_1^\dagger\left[\frac{s_1}{2}\right] D_2^\dagger\left[\frac{s_2}{2}\right] \right. \\ &\quad \left. + B_+ D_1^\dagger\left[\frac{s_1}{2}\right] D_2\left[\frac{s_2}{2}\right] + B_- D_1\left[\frac{s_1}{2}\right] D_2^\dagger\left[\frac{s_2}{2}\right] \right\} |\phi\rangle, \quad (11) \end{aligned}$$

where $\kappa = 1/\sqrt{P_s}$ is the normalization factor and $P_s = \langle\tilde{\Phi}|\tilde{\Phi}\rangle$ denotes the post-selection success probability, $A_\pm = (\hat{I} \pm \langle\hat{\sigma}_x\rangle_w)(\hat{I} \pm \langle\hat{\sigma}_y\rangle_w)$ and $B_\pm = (\hat{I} \mp \langle\hat{\sigma}_x\rangle_w)(\hat{I} \pm \langle\hat{\sigma}_y\rangle_w)$, with the weak value (WV) $\langle\hat{\sigma}_x\rangle_w$ and $\langle\hat{\sigma}_y\rangle_w$ given by

$$\langle\hat{\sigma}_x\rangle_w = \frac{\langle\psi_f|\hat{\sigma}_x|\psi_i\rangle}{\langle\psi_f|\psi_i\rangle} = e^{i\delta_1} \tan\left(\frac{\theta_1}{2}\right). \quad (12)$$

$$\langle\hat{\sigma}_y\rangle_w = \frac{\langle\psi_f|\hat{\sigma}_y|\psi_i\rangle}{\langle\psi_f|\psi_i\rangle} = -ie^{i\delta_2} \tan\left(\frac{\theta_2}{2}\right). \quad (13)$$

Here the parameters satisfy $\delta_j \in [0, 2\pi]$, $\theta_j \in [0, \pi]$ for $j = 1, 2$. For concreteness, we consider two separate pre-selection settings: one for $\langle\hat{\sigma}_x\rangle_w$ and one for $\langle\hat{\sigma}_y\rangle_w$. The weak values (WV) are generally complex. Equations (12) and (13) show that when the pre-selected $|\psi_i\rangle$ and post-selected states $|\psi_f\rangle$ are nearly orthogonal, the weak values can become large, leading to weak-value amplification (WVA) [29]. It is worth noting that the weak value is inherently a product of the two-state vector formalism (TSVF) [30, 31], where the system is characterized by both a pre-selected state evolving forward in time and a post-selected state evolving backward. Within this framework, the weak value is solely determined by the choice of pre- and post-selected states, independent of the measurement strength [21, 32–34]. Hence, contrary to what the name "weak value" might imply, its existence does not require a weak interaction. It remains a well-defined quantity across the entire spectrum of measurement strengths, from the weak-coupling limit all the way to projective measurements

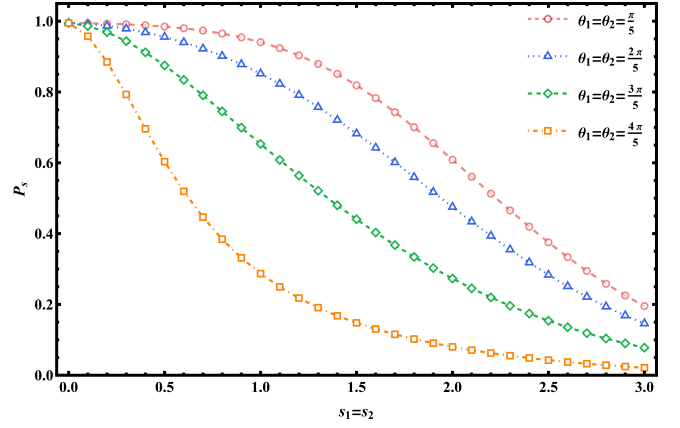


Figure 2. Post-selection success probability P_s of the state $|\Phi\rangle$ as a function of the coupling strength s_i for different weak-value parameters. Fixed parameters are $\mu = 0$, $\varphi = \delta_1 = \delta_2 = \pi/2$, and $r = 0.1$.

[35–37]. This understanding has been experimentally verified in various platforms, demonstrating that weak values can be extracted even under strong measurement conditions using appropriate projective measurements and phase rotations [38].

As shown in Fig. 2, the final pointer state $|\Phi\rangle$ depends on both the WV and the coupling strengths. The success probability P_s decreases as the weak value increases in the weak-measurement regime. However, larger coupling coefficients s_1 and s_2 can, in some parameter regimes, partially compensate for the reduced success probability associated with anomalous weak values, which are typically associated with low post-selection probabilities.

It is important to emphasize that the final pointer state $|\Phi\rangle$ is obtained without using the first-order Aharonov–Albert–Vaidman (AAV) approximation [32, 33]. We retain the finite-coupling unitary evolution and evaluate the post-selected pointer state directly. This treatment allows the parameters s_1 and s_2 to be explored in a weak-to-intermediate coupling regime, rather than being restricted to the strict infinitesimal-coupling limit. As a result, the weak values $\langle\hat{\sigma}_x\rangle_w$ and $\langle\hat{\sigma}_y\rangle_w$ remain the quantities determined by the chosen pre- and post-selected states, and the post-selection back action can be analyzed beyond the simplest AAV linear-response picture. In summary, this work provides a general framework in which PVMs act as a tunable mechanism for modifying the nonclassical properties and metrological performance of ECS.

In the following sections, we examine the specific effects that anomalous WV of the measured system observable exert on the intrinsic properties of $|\Phi\rangle$.

III. EFFECTS ON SQUEEZING

In this section, we examine the influence of PVMs on the squeezing properties of ECS by considering both quadrature squeezing (QS) and sum squeezing (SS).

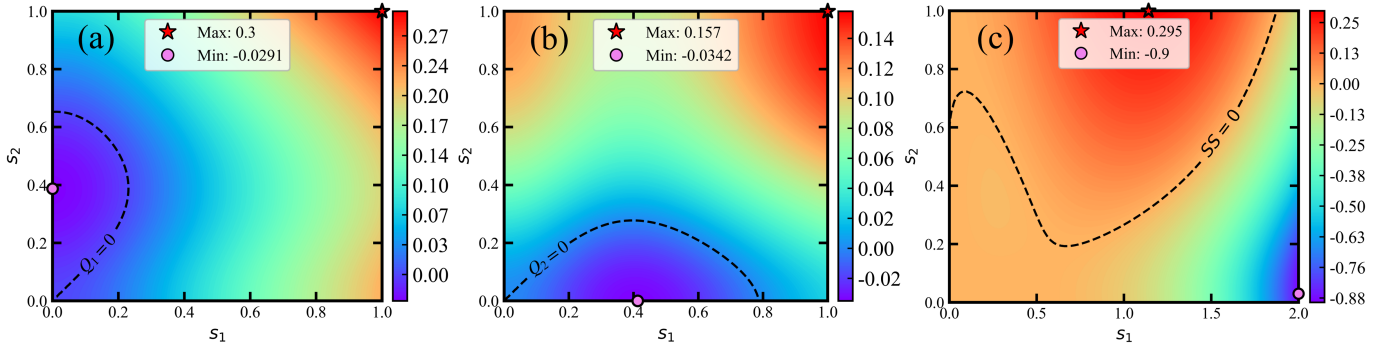


Figure 3. Squeezing parameters in the $s_1 - s_2$ plane: (a) Q_1 squeezing, (b) Q_2 squeezing, and (c) Sum squeezing in the state $|\Phi\rangle$ as functions of the coupling strengths s_1 and s_2 . Fixed parameters are $\mu = \varphi = \Theta = \delta_1 = \delta_2 = \pi/2$, $\theta_1 = \theta_2 = 4\pi/5$, and $r = 0.1$.

A. Quadrature Squeezing

Squeezing is a hallmark of nonclassicality in quantum optics. It arises from the redistribution of quadrature fluctuations, allowing one quadrature to fall below the standard quantum limit [39, 40]. We investigate this effect for ECS under PVNMs.

We first introduce a pair of quadrature operators defined as

$$\hat{F}_1 = (\hat{a} + \hat{b} + \hat{a}^\dagger + \hat{b}^\dagger)/2^{3/2}, \quad (14)$$

$$\hat{F}_2 = (\hat{a} + \hat{b} - \hat{a}^\dagger - \hat{b}^\dagger)/i2^{3/2}, \quad (15)$$

where \hat{a} and \hat{b} represent annihilation operators for two distinct spatial modes, with their Hermitian conjugates denoting the corresponding creation operators. These operators characterize a pair of orthogonal variables in phase space. They obey the commutation relation $[\hat{F}_1, \hat{F}_2] = i/2$, which leads directly to the uncertainty relation

$$\Delta\hat{F}_1^2 \Delta\hat{F}_2^2 \geq 1/16. \quad (16)$$

Here, $\Delta\hat{F}_i^2 = \langle \hat{F}_i^2 \rangle - \langle \hat{F}_i \rangle^2$ denotes the quantum fluctuation of the i th quadrature component. To quantify the degree of squeezing, we define a squeezing parameter as

$$Q_i = \Delta\hat{F}_i^2 - 1/4, \quad (17)$$

where $1/4$ corresponds to the noise level of a coherent state, the standard quantum limit for a minimum uncertainty state. When $-1/4 < Q_i < 0$, the state is squeezed along that quadrature, indicating fluctuations below the coherent-state level. The theoretical lower bound $Q_i = -1/4$ corresponds to perfect squeezing, where the variance vanishes entirely. After algebraic simplification, the orthogonal squeezing parameter Q_i of $|\Phi\rangle$ can be written as

$$Q_1 = \frac{1}{4} [\langle \hat{a}^\dagger \hat{a} \rangle + \langle \hat{b}^\dagger \hat{b} \rangle + \text{Re}[\langle \hat{a}^2 \rangle + \langle \hat{b}^2 \rangle]] + \frac{1}{2} \text{Re}[\langle \hat{a} \hat{b} \rangle] + \frac{1}{2} \text{Re}[\langle \hat{a}^\dagger \hat{b} \rangle] - \frac{1}{2} [\text{Re}[\langle \hat{a} \rangle] + \text{Re}[\langle \hat{b} \rangle]]^2. \quad (18)$$

and

$$Q_2 = \frac{1}{4} [\langle \hat{a}^\dagger \hat{a} \rangle + \langle \hat{b}^\dagger \hat{b} \rangle - \text{Re}[\langle \hat{a}^2 \rangle + \langle \hat{b}^2 \rangle]] - \frac{1}{2} \text{Re}[\langle \hat{a} \hat{b} \rangle] - \frac{1}{2} \text{Re}[\langle \hat{a}^\dagger \hat{b} \rangle] - \frac{1}{2} [\text{Im}[\langle \hat{a} \rangle] + \text{Im}[\langle \hat{b} \rangle]]^2. \quad (19)$$

Here $\langle \cdot \rangle$ denotes expectation values taken with respect to the states $|\phi\rangle$ and $|\Phi\rangle$. A direct calculation for $|\phi\rangle$ shows that the ECS exhibit no squeezing in the two orthogonal directions $Q_{1,\phi} = Q_{2,\phi} = 0$. We then computed Q_1 and Q_2 for the state $|\Phi\rangle$ and plotted their dependence on s_1 and s_2 in Fig. 3 to illustrate the trends. As shown in Fig. 3(a), $Q_1 < 0$ in the plotted region, indicating quadrature squeezing below the coherent-state level. More importantly, Fig. 3(b) exhibits a distinct, though narrow, region of negative values at small s_2 and intermediate s_1 . That negative value corresponds to a measurable reduction of fluctuations below the standard quantum limit and demonstrates that phase-sensitive post-selection can produce quadrature squeezing. The effect is directional and parameter selective; by tuning the coupling strengths and relative phases, the squeezed regime can be accessed reproducibly. The magnitude of the squeezing is modest, but its rapid appearance and disappearance with s_1 and s_2 point to clear operating conditions for optimization.

Overall, the comparison between Figs. 3(a) and 3(b) shows that post-selection induced interference provides a practical and tunable route to generate quadrature squeezing with modest resources, suitable for proof-of-principle demonstrations and for applications that can exploit small, reliably produced reductions in noise.

B. Sum squeezing

In this subsection, we investigate how PVNMs influence the squeezing properties of ECS, focusing on SS. This quantity, first introduced by Hillery [41], serves as a sensitive indicator of nonclassical correlations in two-mode radiation fields. It is defined as follows:

$$V_\Theta = \frac{1}{2} (e^{i\Theta} \hat{a}^\dagger \hat{b}^\dagger + e^{-i\Theta} \hat{a} \hat{b}), \quad (20)$$

Here, $\Theta \in [0, 2\pi]$ defines the rotation angle of V_Θ relative to the real axis in the complex plane [41–44]. A state is said to be SS for a value of Θ if $\langle V_\Theta^2 \rangle - \langle V_\Theta \rangle^2 < \langle N_a + N_b + 1 \rangle / 4$, where $N_a = \hat{a}^\dagger \hat{a}$ and $N_b = \hat{b}^\dagger \hat{b}$, then we can define the degree of SS in the following manner

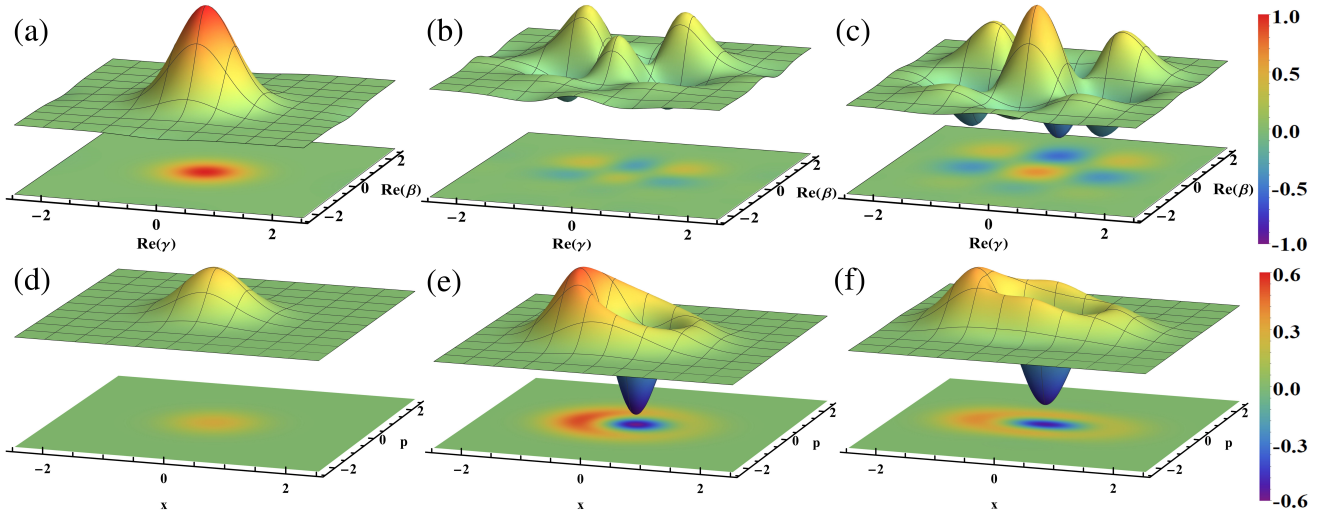


Figure 4. (a)-(c): Real-axis cross sections ($\text{Im } \gamma = \text{Im } \beta = 0$) of the joint quasiprobability $P_J(\gamma, \beta)$ in the $\text{Re } \gamma - \text{Re } \beta$ plane for $s_1 = s_2 = 0, 1, 2$. (d)-(f): single-mode Wigner $W(x, p)$ of the reduced state for $s_2 = 0$ and $s_1 = 0, 1, 2$, respectively. Other parameters are the same as in Fig. 3.

$$SS = \frac{4(\langle V_\Theta^2 \rangle - \langle V_\Theta \rangle^2)}{\langle N_a + N_b + 1 \rangle} - 1. \quad (21)$$

For $-1 \leq SS < 0$, the two-mode state exhibits squeezing, with the squeezing strength increasing as SS approaches -1 . Substituting Eq. (20) into Eq. (21) yields an expression for SS in normally ordered operator form

$$SS = \frac{2[\text{Re}[e^{-2i\Theta}\langle \hat{a}^2 \hat{b}^2 \rangle] - 2(\text{Re}[e^{-i\Theta}\langle \hat{a} \hat{b} \rangle])^2 + \langle N_a N_b \rangle]}{\langle N_a \rangle + \langle N_b \rangle + 1}. \quad (22)$$

Here, $\langle \cdot \rangle$ indicates the expectation value evaluated in $|\Phi\rangle$. Setting $s_1 = s_2 = 0$ recovers the ECS inherent $SS = 0$. As shown in Fig. 3(c), the total squeezing parameter undergoes a continuous evolution from negative to positive values, with the corresponding coupling coefficients s_1 and s_2 varying accordingly. Within the regime of weakly coupled systems, the system primarily exhibits behaviour that is anti-squeezed. As coupling coefficients s_1 and s_2 increase, the system undergoes a gradual transition into an enhanced squeezing state. It is noteworthy that when s_2 is constrained within the weaker region, the magnitude of s_1 is found to exhibit a substantial amplification in its quantum properties. This result demonstrates that quantum squeezing behaviour can be effectively manipulated by regulating the coupling strength, enabling flexible switching between squeezed and anti-squeezed states. This property is of considerable significance for the preparation of nonclassical light fields and parameter optimisation in the domain of quantum information processing. To further support these conclusions, the ensuing discourse employs the joint Wigner function as a fundamental tool for validation.

IV. MEASUREMENT BACKACTION IN PHASE SPACE

A. Joint Wigner function

To investigate the effect of PVNMs on the initial pointer state $|\phi\rangle$, we analyze the phase-space distribution of the post-measurement state $|\Phi\rangle$ through its Wigner function. The joint Wigner function of the two-mode state $|\Phi\rangle$ is defined as

$$\begin{aligned} W_J(\gamma, \beta) &= \frac{4}{\pi^2} \text{Tr}[\rho_{ab} D(\gamma) D(\beta) P_J D^\dagger(\beta) D^\dagger(\gamma)] \\ &= \frac{4}{\pi^2} P_J(\gamma, \beta), \end{aligned} \quad (23)$$

where $\rho_{ab} = |\Phi\rangle\langle\Phi|$ is the density operator of state $|\Phi\rangle$, and $P_J = P_a P_b = \exp[i\pi a^\dagger a + i\pi b^\dagger b]$ is the joint photon number parity operator. The operators $D(\gamma) = \exp[\gamma a^\dagger - \gamma^* a]$ and $D(\beta) = \exp[\beta b^\dagger - \beta^* b]$ are the displacement operators acting on the a and b -modes of the two-mode state $|\Phi\rangle$, respectively. The joint Wigner function W_J describes the state in a four-dimensional (4D) phase space with coordinates $(\text{Re}(\gamma), \text{Im}(\gamma), \text{Re}(\beta), \text{Im}(\beta))$. For the phase-space analysis of the state $|\Phi\rangle$, we use the scaled Wigner function $P_J(\gamma, \beta)$, with

$$-1 \leq P_J(\gamma, \beta) \leq 1. \quad (24)$$

To highlight the key characteristics of the 4D Wigner function for the state $|\Phi\rangle$ and to compare it with the initial state $|\phi\rangle$, we begin by presenting 2D cross-sections along the $\text{Re}(\gamma)$ and $\text{Re}(\beta)$ plane of the joint Wigner function. From Figs. 4(a), 4(b), and 4(c), it can be observed that the joint Wigner function $P_J(\gamma, \beta)$ exhibits significant structural evolution with variations in the coupling strength. When $s_1 = s_2 = 0$, the distribution assumes a concentrated symmetric form with a limited range of negative values, indicating weaker nonclassical properties in the system. As the parameters increase to $s_1 = s_2 = 1$,

the joint distribution develops a multi-branch structure with a markedly enhanced negative region, indicating a pronounced quantum interference effect. Under strong coupling conditions $s_1 = s_2 = 2$, the negative region further expands to form intricate interference fringes, reflecting the system's highly nonclassical behaviour and multi-mode quantum correlations.

Given that the joint Wigner function faithfully reflects the underlying structure of a quantum state, it is well suited for probing changes induced by measurement. From this perspective, a detailed examination of how the phase-space distribution of the a mode evolves in the pointer state $|\Phi\rangle$ after PVMs becomes essential for clarifying how the intrinsic features of the ECS are affected.

B. Wigner function

The Wigner function for the reduced single-mode state $\hat{\rho}_a = \text{Tr}_b[|\Phi\rangle\langle\Phi|]$ is given by [25]

$$W(x, p) = \frac{1}{\pi^2} \iint_{-\infty}^{\infty} e^{2i(p\lambda' - x\lambda'')} \text{Tr}[\rho_a e^{\lambda\hat{a}^\dagger - \lambda^*\hat{a}}] d\lambda' d\lambda'', \quad (25)$$

where, $\lambda = \lambda' + i\lambda''$, x , and p to emphasize the analogy between the quadratic radiation field and the normalized dimensionless position and momentum observables of the beam in phase space.

Figures 4(d), 4(e), and 4(f) show the Wigner function $W(x, p)$ for different coupling strengths s_1 . As s_1 increases, the Wigner function peak shifts from phase space center to the edge, with shape becoming increasingly irregular. Compared with the initial state, the post-measurement state develops negative regions in phase space and exhibits a distinct squeezing effect. Both this squeezing effect and the nonclassicality (evidenced by larger and more pronounced negative regions) strengthen as s_1 increases. This indicates that, under appropriate parameters, the measurement significantly enhances the nonclassical characteristics of the pointer state.

Overall, this visualization shows that modulating the coupling strength significantly modifies the nonclassical phase-space features of the pointer state. Building on these results, we employ the Hillery-Zubairy criterion and linear entropy to characterize the influence of PVMs on quantum correlations in ECS.

V. EFFECT OF ENTANGLEMENT

In this section, we study how PVMs modify the quantum correlations of ECS. In particular, we analyze the post-measurement Hillery-Zubairy correlations and the linear-entropy coefficients that appear in several multimode entanglement criteria to elucidate how the measurement process alters quantum-correlation properties.

A. Hillery-Zubairy correlation

To characterize the entanglement between the two modes of the optical field, we begin by employing the Hillery-Zubairy correlation (HZC) [45], defined as follows [46]:

$$E = \langle \hat{a}^\dagger \hat{a} \rangle \langle \hat{b}^\dagger \hat{b} \rangle - |\langle \hat{a} \hat{b} \rangle|^2. \quad (26)$$

This entanglement criterion underscores the significance of the correlation $\langle \hat{a} \hat{b} \rangle$ between the two modes of a state. Negative values of E certify entanglement, whereas positive values do not imply separability. Additionally, the relation $|\langle \hat{a} \hat{b} \rangle|^2 \leq \langle \hat{a}^\dagger \hat{a} \rangle \langle \hat{b}^\dagger \hat{b} \rangle$ [45, 47] holds, yielding the bound that the entanglement condition for two-mode fields is restricted to $-\langle \hat{a}^\dagger \hat{a} \rangle \leq E < 0$. For the initial ECS $|\phi\rangle$ the HZC gives $E_\phi = 0.25|\alpha|^2(1 + \exp[-|\alpha|^2])^{-2}$, the HZC quantity depends on the coherent amplitude $|\alpha|$. Since the HZC serves as an entanglement witness, its value should be interpreted together with its sign: negative values certify entanglement, whereas positive values alone do not imply separability.

We analyze compliance with the HZC for the final pointer state $|\Phi\rangle$ by computing Eq. (26). As shown in Fig. 5, the HZC reveals that the post-selected two-mode entanglement depends sensitively on the WV parameters. The two-dimensional density plot in Fig. 5(a) shows that when the coupling parameters s_1 and s_2 increase synchronously, the criterion quantity E systematically deviates from the classical limit along the $s_1 = s_2$ direction, indicating that nonclassical correlations are enhanced over a wide parameter domain. Fig. 5(b) presents the quantitative behavior of E as the auxiliary parameter s increases under several fixed coupling strengths $s_1 = s_2$, with larger $s_{1,2}$ corresponding to steeper response curves, indicating that WVA can increase the amplitude of the entanglement witness and enhance its sensitivity to changes in system parameters. Fig. 5(c) shows that the WV parameters θ_1 and θ_2 can effectively modulate the amplification amplitude. Specific phase combinations can make the deviation of the criterion more significant, while other phases suppress this effect. In summary, weak measurement and post-selection can redistribute interference weights and thereby modify the observed bipartite quantum correlations. This can enhance entanglement signatures while maintaining continuous control within experimentally accessible coupling and phase parameters [48]. The approach enhances entanglement detectability and offers a controllable route for ECS-based quantum information processing and quantum metrology. These results are further corroborated by linear entropy analysis.

B. Linear entropy

Linear entropy serves as a convenient measure of bipartite entanglement [45], grounded in the established relation between entanglement and the mixedness of reduced states [49–51]. Formally, the linear entropy of a subsystem is given by:

$$E_{\text{lin}} = 1 - \text{Tr}(\rho_a^2) = 1 - \text{Tr}(\rho_b^2), \quad (27)$$

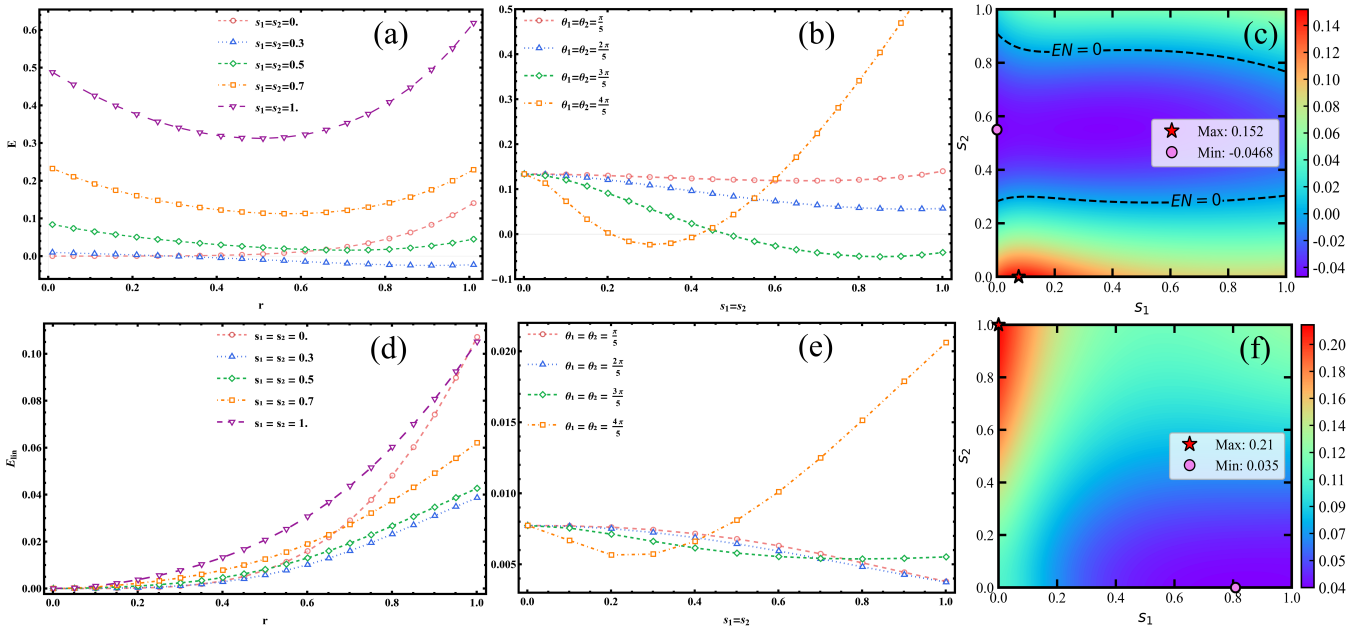


Figure 5. Hillery-Zubairy correlation E and linear entropy E_{lin} for the state $|\Phi\rangle$. Panels (a) and (d) show E and E_{lin} as functions of r for different symmetric couplings $s_1 = s_2$. Panels (b) and (e) show E and E_{lin} as a function of $s_1 = s_2$ for several weak-value parameters at $r = 0.5$. Panels (c) and (f) show E and E_{lin} on the s_1 and s_2 plane at $r = 1$. Other parameters are the same as in Fig. 3.

where $\rho_a = \text{Tr}_b[|\Phi\rangle\langle\Phi|]$ and $\rho_b = \text{Tr}_a[|\Phi\rangle\langle\Phi|]$ denote the reduced density matrices obtained by partial trace over mode a and mode b . This quantity is bounded between 0 and 1, $E_{\text{lin}} = 0$ corresponds to a pure reduced state, indicating separability, while $E_{\text{lin}} \rightarrow 1$ signifies a maximally mixed reduced state, indicating stronger entanglement within the explored parameter regime. Unlike the von Neumann entropy, the linear entropy circumvents the need for diagonalizing the density matrix and can be interpreted as its leading (quadratic) approximation, making it a particularly practical tool for the analysis of non-Gaussian states.

As shown in Figs. 5(d), 5(e), and 5(f), the linear entropy E_{lin} employed as a measure of two-mode entanglement is plotted quantitatively against the system parameter r for several fixed values of the symmetric coupling strength parameter $s_1 = s_2$. The analysis reveals that, for any given coupling strength parameter s_1 and s_2 , the linear entropy E_{lin} increases monotonically with r , confirming that r is the dominant physical parameter driving the generation and growth of quantum entanglement in this setting.

More importantly, at fixed value of r , the linear entropy E_{lin} increases as the coupling strengths s_1 and s_2 are increased. In particular, when $s_1 = s_2 = 1$, the system exhibits the highest degree of entanglement across the whole parameter interval $0 \leq r < 1$. This observation suggests that, in addition to the entanglement-generation mechanism governed by r , applying symmetric and tunable coupling strengths s_1 and s_2 to both modes can enhance the final entanglement resource. Our results provide both a theoretical basis and an experimentally feasible protocol for on-demand control of entanglement in continuous-variable systems [52], realized through composite parameter tuning and squeezing operations.

VI. CRAMÉR-RAO BOUND

The metrological relevance of post-selected weak measurement lies in whether the post-selected state can improve phase-estimation precision. To investigate this, we employ the Quantum Fisher Information (QFI) as our core tool. Entangled coherent states have been shown to provide superior phase sensitivity over NOON and bat states under both ideal and lossy conditions [6]. In that standard ECS metrology, the original ECS outperforms NOON and bat states in the small-photon-number regime and approaches the NOON limit for large photon numbers. Here, we examine whether PVMs can further enhance this performance. As will be shown, the answer is affirmative in the large-average-photon-number regime, albeit with a distinct parameter dependence. The QFI quantifies the ultimate precision limit for estimating an unknown parameter encoded in a quantum state. In the case of a pure quantum state, it is defined as

$$\mathcal{F} = 4[\langle\Phi'|\Phi'\rangle - |\langle\Phi'|\Phi\rangle|^2], \quad (28)$$

with

$$|\Phi'\rangle = \partial|\Phi\rangle/\partial\varphi = \mathcal{N}\chi\alpha e^{i\varphi}\hat{b}^\dagger|0\rangle_a|\alpha e^{i\varphi}\rangle_b, \quad (29)$$

where $\chi = \kappa\{t_+D_1[s_1/2]D_2[s_2/2] + t_-D^\dagger[s_1/2]D^\dagger[s_2/2] + t'_+D^\dagger[s_1/2]D[s_2/2] + t'_-D[s_1/2]D^\dagger[s_2/2]\}/4$. In addition to ECS, we examine the performance of NOON state ($|\psi_N\rangle$) and bat state ($|\psi_B\rangle$) [53]. The uncertainty in estimating the parameter φ is lower-bounded by the Quantum Cramér-Rao bound (QCRB):

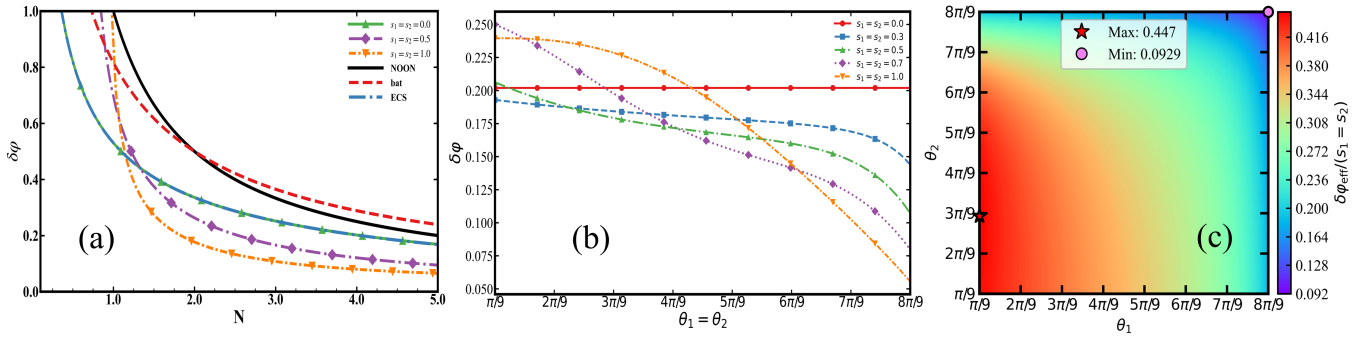


Figure 6. Quantum Cramér-Rao bound $\delta\varphi$ for the state $|\Phi\rangle$. (a) $\delta\varphi$ versus N for $s_1 = s_2 = 0, 0.5, 1$, and $\theta_1 = 8\pi/9$, $\theta_2 = \pi/9$, with NOON, bat, and ECS states as references. (b) $\delta\varphi$ versus $\theta_1 = \theta_2$ for $s_1 = s_2 = 0$ to 1. (c) $\delta\varphi_{\text{eff}}$ versus θ_1, θ_2 at $s_1 = s_2 = 0.5$. Fixed parameters are $\mu = \varphi = \delta_1 = \delta_2 = \pi/2$.

$$\delta\varphi \geq \frac{1}{\sqrt{\mu\mathcal{F}}}. \quad (30)$$

Here, μ represents the total number of independent measurements, where $\mu = 1$ corresponds to a single-shot experiment [5, 54]. For a fair comparison of phase-estimation performance, we take the total mean photon number N as the resource metric. For a two-mode state, the mean photon number in each mode is

$$\langle \psi_k | a^\dagger a | \psi_k \rangle = N/2 = \mathcal{N}^2 |\alpha|^2. \quad (31)$$

Here, we consider four representative states, denoted by $|\psi_k\rangle$ with $k = N, B, E$ and $|\Phi\rangle$, such that the total mean photon number of the system is N , the phase uncertainty $\delta\varphi$ becomes a function of N . Considering the situation with no loss, the optimal phase estimation of the pure states is analytically soluble, yielding $\delta\varphi_N \geq 1/N$ for the NOON state, $\delta\varphi_B \geq 1/\sqrt{N(N/2+1)}$ for the bat state, and for the ECS $\delta\varphi_E \geq 1/2\alpha\mathcal{N}\{1 + [1 - (N\alpha)^2]\alpha^2\}^{1/2}$, thereby enabling a direct resource-based comparison, with detailed derivations given in Appendix A.

To quantify the overall metrological performance beyond the conditional post-selected channel, it is useful to introduce an effective figure of merit that accounts for the post-selection probability. The QFI and QCRB discussed above refer to the successful post-selected subensemble. Therefore, the apparent metrological enhancement should be interpreted together with the post-selection success probability P_s , since only a fraction of the initial trials contributes to the accepted outcomes. A natural effective figure of merit for the full protocol is the success-probability-weighted QFI, $\mathcal{F}_{\text{eff}} = P_s \mathcal{F}_{\text{post}}$, which leads to the effective bound

$$\delta\varphi_{\text{eff}} \geq \frac{1}{\sqrt{\mu\mathcal{F}_{\text{eff}}}}. \quad (32)$$

This effective figure of merit clarifies the trade-off between metrological enhancement and probabilistic post-selection: a larger conditional QFI does not necessarily imply a better overall

protocol unless the success probability remains sufficiently high. A complete resource accounting therefore requires the joint optimization of F_{post} and P_s .

As shown in Fig. 6(a), it is instructive to compare the performance of our post-selected ECS with that of the standard ECS studied in [6]. In that work, the original ECS was shown to outperform NOON and bat states in the small-photon-number regime and to approach the NOON limit for large photon numbers. Our scheme exhibits a distinctly different trend. As can be seen from Fig. 6(a), for very small average photon numbers the post-selected state does not offer a clear advantage over NOON or bat states. However, for large average photon numbers, the post-selected ECS achieves a significantly lower QCRB than all reference states, including the original ECS, NOON, and bat states. This crossover indicates that the WV-induced reshaping of the pointer state becomes effective only above a threshold photon number, where the post-selection backaction and the associated increase in QFI overcome the intrinsic limitations of the bare ECS. Therefore, PVMs provide a tunable enhancement mechanism that is most beneficial in the large-average-photon-number regime, complementing the advantages of standard ECS metrology. In Fig. 6(b) shows that $\delta\varphi$ decreases as $\theta_1 = \theta_2$ increases, and the improvement becomes more pronounced for larger equal coupling strengths. When $s_1 = s_2 = 0$, the bound remains almost unchanged, whereas nonzero coupling introduces a clear dependence on $\theta_1 = \theta_2$, with the strongest coupling yielding the best phase sensitivity over most of the range. Fig. 6(c) illustrates the effective QCRB in the θ_1 and θ_2 plane for $s_1 = s_2 = 0.5$. The phase sensitivity varies significantly with both angles, with larger values of θ_1 and θ_2 leading to a smaller $\delta\varphi_{\text{eff}}$. The maximum and minimum values are marked by the star and circle, respectively, indicating the parameter region that optimizes the successful post-selected precision.

In summary, we establish the ultimate precision of a phase-estimation protocol using PVMs by applying the QFI and the QCRB. Our analysis reveals that optimizing the ECS can produce a quantum gain similar to that associated with WVA, thereby improving phase sensitivity within the studied regime. This approach reduces the estimation error in the successful post-selected subensemble, suggesting improved phase sensitivity

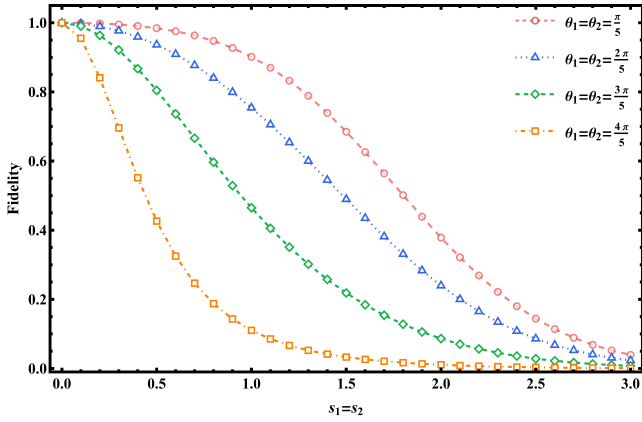


Figure 7. Fidelity $F = |\langle \phi | \Phi \rangle|^2$ as a function of r for different values of $s_1 = s_2$. Other parameters are the same as in Fig. 3.

within the parameter regime considered.

VII. FIDELITY

As discussed above, PVNMs modify the quantum state and thereby influence the nonclassical properties of ECS. To quantify the measurement-induced disturbance, we evaluate the fidelity between the initial pointer state $|\phi\rangle$ and the final state $|\Phi\rangle$. Expressed as:

$$F = |\langle \phi | \Phi \rangle|^2, \quad (33)$$

which satisfies $0 \leq F \leq 1$, with $F = 1$ ($F = 0$) corresponding to identical (orthogonal) states. As shown in Fig. 7, the fidelity decreases monotonically as the dimensionless coupling strengths s_1 and s_2 increase. This behavior reflects an increasing measurement backaction induced by stronger system–pointer coupling, leading to a progressive departure of the post-selected state from the initial pointer configuration. Notably, the behavior holds generally across different WV. However, when the pre- and post-selected states approach orthogonality, anomalously large WV arise.

In particular, when the pre- and post-selected states become nearly orthogonal, giving rise to anomalously large WV, the fidelity decays significantly faster. This behavior highlights the intrinsic trade-off of WVA: enhanced signal sensitivity is accompanied by increased measurement-induced disturbance. This enhanced distinguishability underscores the role of anomalous WV in amplifying the measurement-induced disturbance, leading to a more pronounced departure of the pointer state from its initial configuration. The observed acceleration further illustrates the sensitivity of the measurement back-action to the choice of post-selection, highlighting a key controllability aspect within weak measurement frameworks. Next, we investigate the effects of von Neumann measurement on the quantum state evolution of ECS.

VIII. TIME EVOLUTION AND NEGATIVITY

To frame this analysis, we begin by reviewing the general description of quantum dynamics for a composite system. Typically, such a system is initially prepared in a separable state of the form

$$\rho_{in} = |\psi_i\rangle\langle\psi_i| \otimes |\phi\rangle\langle\phi|, \quad (34)$$

where the subsystem and probe are uncorrelated at $t = 0$. Its unitary evolution follows [55]

$$\rho_{after} = U(t)\rho_{in}U^\dagger(t), \quad (35)$$

where $U(t)$ is the evolution operator defined in Sec. II. After the system–pointer interaction, applying the post-selection operator $\Pi = |\psi_f\rangle\langle\psi_f| \otimes \mathbb{I}$ yields the unnormalized pointer density operator $\tilde{\rho} = \Pi\rho_{after}\Pi$, whose trace gives the post-selection success probability $\text{Tr}[\tilde{\rho}]$, and the normalized post-selected state is

$$\rho(\tau = 0) = \frac{\tilde{\rho}}{\text{Tr}[\tilde{\rho}]}. \quad (36)$$

Here, τ represents the physical evolution time, and $\rho(\tau = 0)$ defined the initial condition. To systematically study the time evolution of the density matrix, we introduce the Lindblad master equation under the interaction picture[56–58], expressed as:

$$\partial_\tau \rho(\tau) = \mathcal{L}[\rho(\tau)] = \mathcal{L}_{H_{int}}[\rho(\tau)] + \mathcal{L}_D[\rho(\tau)]. \quad (37)$$

Here, the Liouvillian superoperator \mathcal{L} is composed of the interaction Hamiltonian $\mathcal{L}_{H_{int}}[\rho(\tau)]$ and dissipation $\mathcal{L}_D[\rho(\tau)]$. Hamiltonian evolution term:

$$\mathcal{L}_{H_{int}}[\rho(\tau)] = -i[H_{int}, \rho(\tau)], \quad (38)$$

and dissipation term:

$$\mathcal{L}_D[\rho(\tau)] = \sum_{m=a,b} \gamma_m (L_m \rho(\tau) L_m^\dagger - \frac{1}{2} \{L_m^\dagger L_m, \rho(\tau)\}), \quad (39)$$

where $\{\hat{A}, \hat{B}\} = \hat{A}\hat{B} + \hat{B}\hat{A}$ denotes the anticommutator. We consider two optical modes independently coupled to Markovian loss channels, with jump operators $L_a = \sqrt{\gamma_a}\hat{a}$ and $L_b = \sqrt{\gamma_b}\hat{b}$, where γ_a and γ_b denote the dissipation rates of modes a and b, respectively. These operators describe photon loss processes in the two modes and model the coupling between the ECS and its surrounding environment, with detailed derivations given in Appendix B.

Within this dynamical framework, we investigate how environmental dissipation influences the evolution of the ECS and its entanglement properties. In particular, the resulting density matrix is used to evaluate the entanglement negativity, allowing us to characterize the robustness of the ECS under realistic loss conditions.

Negativity is a widely used entanglement measure for bipartite systems, defined in terms of the partial transpose of the

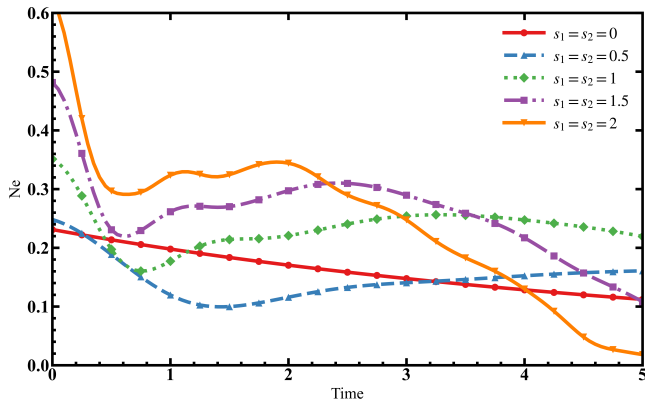


Figure 8. Time evolution of the negativity N_e for different coupling strengths $s_1 = s_2$. Here, $\gamma_a = \gamma_b = 0.1$. Other parameters are the same as in Fig. 3.

density matrix. For a bipartite system $\hat{\rho}_{ab}$, the negativity is defined as

$$N_e = \frac{\|\rho_{ab}^{T_a}\|_1 - 1}{2}, \quad (40)$$

Here, $\rho_{ab}^{T_a}$ represents the partial transpose of mode a , and $\|\cdot\|_1$ denotes the trace norm. A larger value indicates stronger entanglement, while zero indicates no detectable entanglement.

As shown in Fig. 8, the dynamics reveal an interplay between the initial entanglement and the coupling-induced modification of entanglement. When $s_1 = s_2 = 0$, owing to the dynamical evolution of the open quantum system, the negativity shows a slight reduction before stabilizing near 0.18 ± 0.3 . In the absence of coupling, the subsystems evolve independently, and the initial entanglement is preserved, producing a horizontal line. For $s_1 = s_2 = 0.5$, the entanglement starts at 0.25 and exhibits slow, small-amplitude damped oscillations. The weak coupling is insufficient to generate substantial new entanglement and instead perturbs the initial state, leading to slight reductions and fluctuations. At $s_1 = s_2 = 1$, the dynamics develop large-amplitude oscillations, showing that the coupling has become strong enough to drive pronounced entanglement oscillations, further increases in s_1 and s_2 shift the oscillation mean upward. In particular, for $s_1 = s_2 = 2$, the entanglement remains at a high level for most of the evolution, indicating that strong coupling both produces additional entanglement and strongly perturbs the initial entanglement, yielding rapid, high-intensity dynamical behavior.

Overall, building upon the existing entanglement in the system of ECS, increasing the coupling strength transforms the system from a static state to large-amplitude, sustained oscillations, with both the oscillation frequency and the average entanglement level increasing with stronger coupling.

IX. CONCLUSION AND REMARKS

In this work, we investigate how post-selected measurement influences the nonclassical properties of an entangled coherent

state. Focusing on post-selected von Neumann measurements applied to two-mode entangled coherent states, we develop a theoretical framework to analyze how measurement back-action affects their quantum properties. By tuning the system-pointer coupling strength, we show that the measurement process can modify nonclassical features and, in selected parameter regimes, enhance squeezing, Wigner negativity, and bipartite correlations. These changes are accompanied by improved phase-estimation performance in the successful post-selected channel, as indicated by increased quantum Fisher information and a reduced quantum Cramér–Rao bound, while also revealing a trade-off with state fidelity. Notably, unlike the standard ECS metrology which excels in the small-photon-number regime [6], our post-selected scheme delivers its phase-sensitivity advantage specifically for large average photon numbers. Our results suggest that measurement back-action can serve as a useful mechanism for engineering quantum resources in continuous-variable systems and provide a framework for exploring quantum sensing protocols beyond conventional measurement schemes.

Future work should further examine the trade-off among post-selection success probability, state fidelity, and quantum Fisher information in order to identify parameter regimes in which a clear metrological advantage may emerge [20, 59]. In parallel, it is important to extend the present framework to non-Gaussian and hybrid quantum states, where measurement-induced effects may further enhance nonclassical features and sensing performance [60]. In addition, integrating PVNMs with quantum control and error mitigation strategies, such as coherent feedback and reservoir engineering, may provide a route to improve the stability and robustness of the enhanced quantum states in realistic sensing scenarios [61, 62].

X. ACKNOWLEDGMENTS

The computational work in this study, from mathematical derivations to visualizations, was carried out using version 14.3 of the Wolfram Language and the Wolfram Quantum Framework. This work was supported by the National Natural Science Foundation of China (Grant No. 12365005).

Appendix A: Derivation of the Cramér–Rao bounds for the NOON, bat, and entangled coherent states

In this appendix, we derive the Cramér–Rao bounds for the NOON, bat, and entangled coherent states discussed in the main text. The phase to be estimated is encoded in mode b via the unitary transformation $U(\phi) = e^{i\phi n_b}$. For a pure probe state $|\psi(\phi)\rangle$, the quantum Fisher information is $F_Q = 4(\langle \partial_\phi \psi | \partial_\phi \psi \rangle - |\langle \psi | \partial_\phi \psi \rangle|^2)$, and the corresponding phase sensitivity obeys the quantum Cramér–Rao bound $\delta\phi \geq 1/\sqrt{F_Q}$. In the present phase-encoding scheme, the QFI reduces to four times the variance of $n_b = b^\dagger b$, namely, $F_Q = 4 \text{Var}(n_b) = 4(\langle n_b^2 \rangle - \langle n_b \rangle^2)$.

1. Complete derivation for the NOON state

The NOON state is $|\text{NOON}\rangle = (|N, 0\rangle + |0, N\rangle)/\sqrt{2}$. Since mode a and b contains either 0 or N photons with equal probability, we have $\langle n_b \rangle = N/2$ and $\langle n_b^2 \rangle = N^2/2$. Hence

$$\text{Var}(n_a) = \langle n_b^2 \rangle - \langle n_b \rangle^2 = \frac{N^2}{2} - \frac{N^2}{4} = \frac{N^2}{4}. \quad (\text{A1})$$

The quantum Fisher information is therefore $F_Q^N = 4 \text{Var}(n_b) = N^2$, and the QCRB becomes

$$\delta\varphi_N = \frac{1}{N}. \quad (\text{A2})$$

2. Complete derivation for the bat state

For even N , write $N = 2j$. The bat states can be represented by a two-mode Dickie as

$$|B_N\rangle = \sum_{k=0}^{N/2} \frac{\sqrt{(N-2k)!(2k)!}}{k!(N/2-k)!\sqrt{2^N}} |N-2k\rangle_1 |2k\rangle_2. \quad (\text{A3})$$

This state is equivalently the $\pi/2$ -rotation of the Dicke state $|j, 0\rangle$ in the Schwinger representation, $|B_N\rangle = e^{-i(\pi/2)J_y} |j, 0\rangle$, with $J_z = (n_1 - n_2)/2$, and $n_b = j - J_z$. Because $n_a = j + J_z$, the variance of n_b is the same as the variance of J_z :

$$\text{Var}(n_a) = \text{Var}(J_z). \quad (\text{A4})$$

We now evaluate the moments in the rotated state. First, $\langle J_z \rangle_B = \langle j, 0 | e^{i(\pi/2)J_y} J_z e^{-i(\pi/2)J_y} |j, 0\rangle = \langle j, 0 | J_x |j, 0\rangle = 0$. Next, $\langle J_z^2 \rangle_B = \langle j, 0 | J_x^2 |j, 0\rangle$. Using $J_x = (J_+ + J_-)/2$, we have $J_x^2 = (J_+ J_- + J_- J_+ + J_+^2 + J_-^2)/4$. When sandwiched between $\langle j, 0 |$ and $|j, 0\rangle$, the terms J_+^2 and J_-^2 do not contribute, so $\langle j, 0 | J_x^2 |j, 0\rangle = \langle j, 0 | J_+ J_- + J_- J_+ |j, 0\rangle/4$. Using the identity $J_+ J_- + J_- J_+ = 2(J^2 - J_z^2)$, we obtain $\langle J_z^2 \rangle_B = \langle j, 0 | J^2 - J_z^2 |j, 0\rangle/2$. Since $J^2 |j, 0\rangle = j(j+1) |j, 0\rangle$ and $J_z |j, 0\rangle = 0$, this gives $\langle J_z^2 \rangle_B = j(j+1)/2$. Therefore $\text{Var}(n_2) = \text{Var}(J_z) = j(j+1)/2$. Substituting $j = N/2$, we find

$$\text{Var}(n_b) = \frac{N(N+2)}{8}. \quad (\text{A5})$$

Hence the quantum Fisher information is $F_Q^B = 4 \text{Var}(n_b) = N(N+2)/2 = N[(N/2) + 1]$, and the QCRB becomes

$$\delta\varphi_B = \frac{1}{\sqrt{N[(N/2) + 1]}}. \quad (\text{A6})$$

3. Complete derivation for the ECS

The ECS state is $|\text{ECS}\rangle = \mathcal{N}(|\alpha\rangle_a |0\rangle_b + |0\rangle_a |\alpha\rangle_b)$, with normalization \mathcal{N} . The mean photon number in mode b is

$$\begin{aligned} \langle n_a \rangle &= \mathcal{N}^2 [\langle \alpha, 0 | n_b | \alpha, 0 \rangle + \langle 0, \alpha | n_b | 0, \alpha \rangle] \\ &= \mathcal{N}^2 |\alpha|^2. \end{aligned} \quad (\text{A7})$$

The cross terms vanish because $n|0\rangle = 0$ and $\langle 0|n = 0$. Similarly, using the coherent-state moments $\langle \alpha | n_b | \alpha \rangle = |\alpha|^2$, and $\langle \alpha | n_b^2 | \alpha \rangle = |\alpha|^4 + |\alpha|^2$, we obtain

$$\begin{aligned} \langle n_a^2 \rangle &= \mathcal{N}^2 [\langle \alpha, 0 | n_b^2 | \alpha, 0 \rangle + \langle 0, \alpha | n_b^2 | 0, \alpha \rangle] \\ &= \mathcal{N}^2 (|\alpha|^4 + |\alpha|^2). \end{aligned} \quad (\text{A8})$$

Therefore,

$$\begin{aligned} \text{Var}(n_a) &= \langle n_b^2 \rangle - \langle n_b \rangle^2 \\ &= \mathcal{N}^2 |\alpha|^2 [1 + |\alpha|^2 (1 - \mathcal{N}^2)]. \end{aligned} \quad (\text{A9})$$

The quantum Fisher information is thus

$$F_Q^C = 4\mathcal{N}^2 |\alpha|^2 \left[1 + |\alpha|^2 (1 - \mathcal{N}^2) \right], \quad (\text{A10})$$

and the QCRB is

$$\delta\varphi_C = \frac{1}{2\mathcal{N}|\alpha|\sqrt{1 + |\alpha|^2(1 - \mathcal{N}^2)}}. \quad (\text{A11})$$

Appendix B: Model and dynamical evolution

The system is initialized in the general superposition state $|\psi_i\rangle = \cos(\theta/2)|0\rangle + e^{i\delta} \sin(\theta/2)|1\rangle$. The pointer is prepared in a coherent-state superposition of the form $|\phi\rangle$, the total initial state is therefore $|\Psi_{\text{in}}\rangle = |\psi_i\rangle \otimes |\phi\rangle$. The interaction between the system and the pointer is described by $\hat{H}_{\text{int}} = g_a \hat{\sigma}_x \otimes \hat{P}_x + g_b \hat{\sigma}_y \otimes \hat{P}_y$. The corresponding unitary evolution is $U(t) = e^{-iH_{\text{int}}t}$. After the interaction, the composite state becomes $|\Psi_{\text{after}}\rangle = U(t)|\Psi_{\text{in}}\rangle$. A projective measurement is performed on the system, postselecting onto a target state $|\psi_f\rangle$. The projector is

$$\Pi_{\text{post}} = |\psi_f\rangle\langle\psi_f| \otimes I. \quad (\text{B1})$$

The unnormalized post-selected state is $|\tilde{\Psi}_{\text{post}}\rangle = \Pi_{\text{post}}|\Psi_{\text{after}}\rangle$. The success probability reads $P_s = \langle \tilde{\Psi}_{\text{post}} | \tilde{\Psi}_{\text{post}} \rangle$. The normalized c-selected state is $|\Psi_{\text{post}}\rangle = |\tilde{\Psi}_{\text{post}}\rangle/\sqrt{P_s}$. After post-selection, the system undergoes dissipative evolution described by the Lindblad master equation. The dissipation channels are modeled by the Lindblad operators $L_a = \sqrt{\gamma_a}a$, and $L_b = \sqrt{\gamma_b}b$, where γ_a and γ_b are decay rates. The density operator $\rho(\tau)$ satisfies

$$\frac{d\rho}{d\tau} = -i[H_{\text{int}}, \rho] + \sum_{j=a,b} (L_j \rho L_j^\dagger - \{L_j^\dagger L_j, \rho\}/2), \quad (\text{B2})$$

with initial condition $\rho(0) = |\Psi_{\text{post}}\rangle\langle\Psi_{\text{post}}|$. To evaluate the entanglement between the two pointer modes, we trace out the system degrees of freedom, $\rho_{\text{ptr}}(\tau) = \text{Tr}_s[\rho(\tau)]$. We then compute the entanglement negativity via partial transposition,

$$N_e(\tau) = \frac{\left\| \rho_{\text{ptr}}^{T_a}(\tau) \right\|_1 - 1}{2}, \quad (\text{B3})$$

where T_a denotes partial transpose with respect to subsystem a .

- [1] V. Giovannetti, S. Lloyd, and L. Maccone, *Phys. Rev. Lett.* **96**, 010401 (2006).
- [2] Y. Chu, X. Li, and J. Cai, *Phys. Rev. Lett.* **130**, 170801 (2023).
- [3] H. S. Eisenberg, J. F. Hodelin, G. Khoury, and D. Bouwmeester, *Phys. Rev. Lett.* **94**, 090502 (2005).
- [4] K. J. Resch, K. L. Pregnell, R. Prevedel, A. Gilchrist, G. J. Pryde, J. L. O'Brien, and A. G. White, *Phys. Rev. Lett.* **98**, 223601 (2007).
- [5] J. J. Cooper, D. W. Hallwood, and J. A. Dunningham, *Phys. Rev. A* **81**, 043624 (2010).
- [6] J. Joo, W. J. Munro, and T. P. Spiller, *Phys. Rev. Lett.* **107**, 083601 (2011).
- [7] B. C. Sanders, *Phys. Rev. A* **45**, 6811 (1992).
- [8] H. Jeon, J. Kang, J. Kim, W. Choi, K. Kim, and T. Kim, *Sci. Rep* **14**, 6847 (2024).
- [9] I. M. Duck, P. M. Stevenson, and E. C. G. Sudarshan, *Phys. Rev. D* **40**, 2112 (1989).
- [10] Y. Aharonov and L. Vaidman, *Phys. Rev. A* **41**, 11 (1990).
- [11] Y. Aharonov, D. Z. Albert, and L. Vaidman, *Phys. Rev. Lett.* **60**, 1351 (1988).
- [12] B. de Lima Bernardo, S. Azevedo, and A. Rosas, *Opt. Commun.* **331**, 194 (2014).
- [13] J. Yuanbek, Y.-F. Ren, and Y. Turek, *Phys. Rev. A* **111**, 063707 (2025).
- [14] G. C. Knee and E. M. Gauger, *Phys. Rev. X* **4**, 011032 (2014).
- [15] J. C. Howell, D. J. Starling, P. B. Dixon, P. K. Vudyasetu, and A. N. Jordan, *Phys. Rev. A* **81**, 033813 (2010).
- [16] R. Horodecki, P. Horodecki, M. Horodecki, and K. Horodecki, *Rev. Mod. Phys.* **81**, 865 (2009).
- [17] V. Vedral, *Nat. Phys.* **10**, 256 (2014).
- [18] J. Tavares, *Rev. Ciência Elem* (2023).
- [19] E. Descamps, A. Keller, and P. Milman, *Phys. Rev. Lett.* **136**, 060807 (2026).
- [20] S. Pang and T. A. Brun, *Phys. Rev. Lett.* **115**, 120401 (2015).
- [21] Y. Liu, L. Qin, and X.-Q. Li, *Phys. Rev. A* **106**, 022619 (2022).
- [22] J. von Neumann, *Mathematical Foundations of Quantum Mechanics*, edited by N. A. Wheeler (Princeton University Press, Princeton, 2018).
- [23] J. Joo, K. Park, H. Jeong, W. J. Munro, K. Nemoto, and T. P. Spiller, *Phys. Rev. A* **86**, 043828 (2012).
- [24] Z. M. McIntyre and W. A. Coish, *Phys. Rev. A* **110**, L010602 (2024).
- [25] C. Gerry and P. Knight, *Introductory Quantum Optics* (Cambridge University Press, Cambridge, England, 2004).
- [26] C. C. Gerry, J. Mimih, and A. Benmoussa, *Phys. Rev. A* **80**, 022111 (2009).
- [27] G. Puentes, N. Hermosa, and J. P. Torres, *Phys. Rev. Lett.* **109**, 040401 (2012).
- [28] F. Hong-yi, *Phys. Rev. A* **41**, 1526 (1990).
- [29] J. Dressel, M. Malik, F. M. Miatto, A. N. Jordan, and R. W. Boyd, *Rev. Mod. Phys.* **86**, 307 (2014).
- [30] Y. Aharonov, P. G. Bergmann, and J. L. Lebowitz, *Phys. Rev.* **134**, B1410 (1964).
- [31] Y. Aharonov and L. Vaidman, The two-state vector formalism: An updated review, in *Time in Quantum Mechanics*, edited by J. Muga, R. S. Mayato, and Í. Egusquiza (Springer Berlin Heidelberg, Berlin, Heidelberg, 2008) pp. 399–447.
- [32] S. Wu and Y. Li, *Phys. Rev. A* **83**, 052106 (2011).
- [33] J. Ren, L. Qin, W. Feng, and X.-Q. Li, *Phys. Rev. A* **102**, 042601 (2020).
- [34] Y. Turek, H. Kobayashi, T. Akutsu, C.-P. Sun, and Y. Shikano, *New J. Phys.* **17**, 083029 (2015).
- [35] F. De Zela, *Phys. Rev. A* **105**, 042202 (2022).
- [36] E. Cohen and E. Pollak, *Phys. Rev. A* **98**, 042112 (2018).
- [37] H. F. Hofmann, *New J. Phys.* **14**, 043031 (2012).
- [38] R. Wagner, Z. Schwartzman-Nowik, I. L. Paiva, A. Te'eni, A. Ruiz-Molero, R. S. Barbosa, E. Cohen, and E. F. Galvão, *Quantum Sci. Technol.* **9**, 015030 (2024).
- [39] i. c. v. Bräuer, T. c. v. Opatrný, and P. Marek, *Phys. Rev. Res.* **7**, 033176 (2025).
- [40] X. Heng, L. Zhang, Q. Yin, W. Liu, L. Tang, Y. Zhai, and K. Wei, *Appl. Sci* **15** (2025).
- [41] M. Hillery, *Phys. Rev. A* **40**, 3147 (1989).
- [42] Nguyen Ba An and Vo Tinh, *Phys. Lett. A* **261**, 34 (1999).
- [43] Y. Kurochkin, A. S. Prasad, and A. I. Lvovsky, *Phys. Rev. Lett.* **112**, 070402 (2014).
- [44] G. Ren, W. hai Zhang, and Y. jun Xu, *PHYSICA A*. **520**, 106 (2019).
- [45] M. Hillery and M. S. Zubairy, *Phys. Rev. Lett.* **96**, 050503 (2006).
- [46] L. Dao-ming, *Int. J. Theor. Phys.* **54**, 2289 (2015).
- [47] F. Li, T. Li, and G. S. Agarwal, *Phys. Rev. Res.* **3**, 033095 (2021).
- [48] Z.-D. Li, X. Yuan, X.-F. Yin, L.-Z. Liu, R. Zhang, Y.-Y. Fei, L. Li, N.-L. Liu, X. Ma, H. Lu, Y.-A. Chen, and J.-W. Pan, *Phys. Rev. Res.* **2**, 023047 (2020).
- [49] G. S. Agarwal and A. Biswas, *J. Opt. B: Quantum Semiclass. Opt.* **7**, 350 (2005).
- [50] Q. Sun, H. Nha, and M. S. Zubairy, *Phys. Rev. A* **80**, 020101 (2009).
- [51] H. S. Chuong and T. M. Duc, *J. Phys. B: At. Mol. Opt. Phys.* **56**, 205401 (2023).
- [52] K. Araya-Sossa and M. Orszag, *Phys. Rev. A* **108**, 012432 (2023).
- [53] $|\psi_N\rangle = (|N\rangle_a|0\rangle_b + |0\rangle_a|N\rangle_b)/\sqrt{2}$ and $|\psi_B\rangle = \sum_{k=0}^{N/2} \sqrt{(N-2k)!} \sqrt{(2k)!} / k! (N/2 - k)! \sqrt{2^N} |N-2k\rangle_a |2k\rangle_b$. The bat state is so named because its amplitude distribution resembles the wings of a bat.
- [54] M. Zwierz, C. A. Pérez-Delgado, and P. Kok, *Phys. Rev. Lett.* **105**, 180402 (2010).
- [55] M. Mechler, M. A. Manko, V. I. Manko, and P. Adam, *Quantum Rep.* **7** (2025).
- [56] D. Manzano, *AIP Adv.* **10**, 025106 (2020).
- [57] A. Sander, M. Fröhlich, M. Eigel, J. Eisert, P. Gelß, M. Hintermüller, R. M. Milbradt, R. Wille, and C. B. Mendl, *Nat. Commun.* (2025).
- [58] J. Gu and F. Zhang, *Phys. Rev. E* **112**, 044106 (2025).
- [59] C. Ferrie and J. Combes, *Phys. Rev. Lett.* **112**, 040406 (2014).
- [60] A. Ullah, M. T. Naseem, and O. E. Müstecaplıoğlu, *Phys. Rev. A* **112**, 062601 (2025).
- [61] S. Diehl, A. Micheli, A. Kantian, B. Kraus, H. P. Büchler, and P. Zoller, *Nat. Phys.* **4**, 878 (2008).
- [62] H. M. Wiseman and G. J. Milburn, *Phys. Rev. A* **49**, 4110 (1994).